Dynamics of Ring Cleavage and Substitution in the Reactive Scattering of O(^{3}P) Atoms with C_2H_4S and C_4H_4S Molecules

X. Gao, M. P. Hall, D. J. Smith, and R. Grice*

Chemistry Department, University of Manchester, Manchester M13 9PL, U.K.

Received: September 3, 1996; In Final Form: October 16, 1996[⊗]

Reactive scattering of ground state O(^{3}P) atoms with C_2H_4S and C_4H_4S molecules has been studied at an initial translational energy $E \sim 40$ kJ mol^{-1} using a supersonic beam of O atoms seeded in He buffer gas generated from a microwave discharge source. The center-of-mass angular distribution of SO scattering for O + C_2H_4S is cone-shaped in the backward hemisphere at a scattering angle $\theta \sim 120°$ with respect to the incident O atom direction, while the OC_4H_3S scattering for O + C_4H_4S is nominally isotropic. The O + C_2H_4S reaction disposes a lower fraction ($f' \sim 0.3$) of the total available energy into product translation than the O + C_4H_4S reaction ($f' \sim 0.4$), although the product translational energies are higher by a factor of ∼2 for the more exoergic O + C_2H_4S reaction. The O + C_2H_4S reaction involves cleavage of the three-membered ring of the thiirane molecule, while the O + C_4H_4S reaction involves H atom displacement from the five-membered ring of the thiophene molecule. Both reactions occur on the triplet potential energy surface. The strongly exoergic concerted rupture of the three-membered thiirane ring disposes half the available energy into vibrational excitation of the ethene product molecule compared with only a fraction (∼0.13) being disposed into SO product vibration. The displacement reaction of the five-membered thiophene ring involves O atom addition forming a persistent OC_4H_4S complex with a potential energy barrier to H atom displacement.

Introduction

The nascent vibrational state distribution for SO($^3\Sigma^-$) products in the reaction of ground state O(^{3}P) atoms with thiirane (C_2H_4S) molecules has recently been determined in a laser pump−probe experiment[1] using laser-induced fluorescence detection. An inverted vibrational distribution was observed, and a direct S atom abstraction mechanism was proposed in accord with earlier speculations based on O atom resonance fluorescence measurements,[2] which yield a rate constant $k = 7.2 \times 10^9$ dm^3 mol^{-1} s^{-1} independent of temperature.

$$O(^3P) + C_2H_4S \rightarrow SO(^3\Sigma^-) + C_2H_4 \qquad (1)$$

The rate constant for the reaction of O(^{3}P) atoms with thiophene (C_4H_4S) molecules has been measured in a discharge flow resonance fluorescence experiment,[3] giving a preexponential factor $A = 2.0 \times 10^{10}$ dm^3 mol^{-1} s^{-1} and an activation energy $E_a = 9.4$ kJ mol^{-1}. On the basis of an observed break in the Arrhenius plot for these measurements, it was suggested[2] that two reaction mechanisms corresponding to O atom addition to the S atom and the C=C double bond of the thiophene ring may be operative. However, the five-membered thiophene ring with partial aromatic character[4] is more stable than the strained three-membered thiirane ring, and an H atom substitution pathway analogous to that observed[5,6] for O atoms with benzene molecules might be anticipated

$$O(^3P) + C_4H_4S \rightarrow OC_4H_3S + H \qquad (2)$$

Reactive scattering measurements have been undertaken to investigate the dynamics of ring cleavage and the extent to which reaction proceeds via the triplet potential energy surface[7] rather than undergoing intersystem crossing[6] to the underlying singlet potential energy surface.

Experimental Section

The apparatus was the same as that previously employed in studies[8,9] of O(^{3}P) atoms with alkyl iodide molecules. A supersonic beam of O atoms seeded in He buffer gas was produced from a high-pressure microwave discharge source.[10] The thiirane and thiophene molecule beams issued from a glass nozzle of diameter ∼0.25 mm using stagnation pressures ∼100 mbar maintained by a reservoir at ∼−15 and 25 °C. The velocity distributions of the O atom beam measured by a beam monitor quadrupole mass spectrometer and the molecule beams by the rotatable mass spectrometer detector using cross-correlation time-of-flight analysis[11] yield the peak velocities v_{pk}, full widths at half-maximum intensity v_{wd}, and Mach numbers M quoted in Table 1. No evidence was found for any significant dimerization of molecules in the reactant beams when monitoring their mass spectra with the rotatable detector.

Results

Angular distribution measurements of SO reactive scattering from thiirane molecules yield ∼35 counts s^{-1} against a background ∼250 counts s^{-1}, while OC_4H_3S reactive scattering from thiophene molecules yields ∼40 counts s^{-1} against a background ∼12 counts s^{-1}. The laboratory angular distribution of SO scattering in Figure 1 extends over a wide angular range peaking close to the thiirane beam, while the OC_4H_3S scattering in Figure 2 is confined close to the laboratory centroid distribution shown by a broken curve. The number densities of SO scattering were measured by counting selectively in those short-time channels which contribute significantly to the SO reactive scattering, in order to minimize interference from background signals at low velocity arising from elastic scattering of thiirane molecules. The laboratory velocity distributions of SO flux in Figure 3 and OC_4H_3S in Figure 4 were measured using integration times ∼3000 and ∼600 s, respectively, to gain signal-to-noise ratios ∼11 and ∼14 at the peaks of the distributions. Kinematic analysis of these data was performed

[⊗] Abstract published in *Advance ACS Abstracts,* December 15, 1996.

S1089-5639(96)02692-8 CCC: $14.00

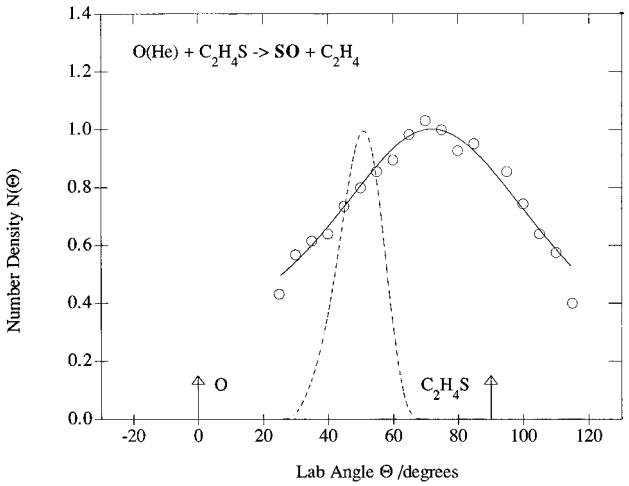

Figure 1. Laboratory angular distribution (number density) of SO reactive scattering from O + C_2H_4S at an initial translational energy $E \sim 41$ kJ mol^{-1}. Solid line shows the fit of the stochastic kinematic analysis, and the broken line shows the distribution of laboratory centroids.

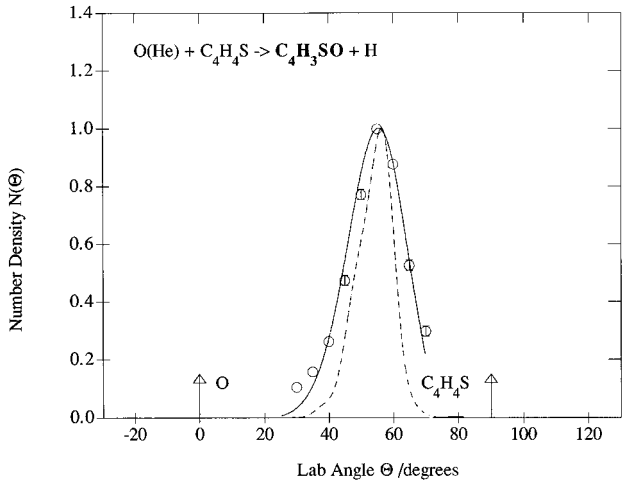

Figure 2. Laboratory angular distribution of OC_4H_3S reactive scattering from O + C_4H_4S at an initial translational energy $E \sim 37$ kJ mol^{-1}.

TABLE 1: Beam Velocity Distributions, Peak Velocity v_{pk}, Full Width at Half-Maximum Intensity v_{wd}, and Mach Number *M*

beam	v_{pk}/m s^{-1}	v_{wd}/m s^{-1}	*M*
O(He)	2450	680	6.5
C_2H_4S	800	430	3.0
O(He)	2250	610	6.5
C_4H_4S	650	270	4.5

using the stochastic method[12] with the differential cross sections expressed as a product of an angular function $T(\theta)$ and a velocity function $U(u)$

$$I_{cm}(\theta,u) = T(\theta)\, U(u) \qquad (3)$$

The resulting angular and product translational energy distributions $P(E')$ are shown for the SO reactive scattering in Figure 5 and OC_4H_3S scattering in Figure 6. The SO angular distribution for O atoms with thiirane molecules shows conical scattering in the backward hemisphere, while the OC_4H_3S angular distribution for O atoms with thiophene molecules is nominally isotropic. The adverse kinematics of the O + C_4H_4S reaction provide only poor resolution of the form of the center-of-mass angular distribution which cannot be distinguished from an isotropic distribution. The product translational energy distribution for SO scattering peaks at a fraction $f' \sim 0.2$ of the total available energy but disposes much higher energy into translation than the OC_4H_3S scattering which peaks at a higher fraction $f' \sim 0.4$ of the much lower energy available to reaction products in this case. The form of the product translational energy distribution is also more poorly resolved for the O + C_4H_4S reaction than for the O + C_2H_4S reaction. The peak E'_{pk} and average E'_{av} product translational energies are listed in Table 2 together with the initial translational energies E and reaction exoergicities ΔD_0, calculated for eq 1 from heats of formation given by Pedley *et al.*[13] and for eq 2 being equated to that of the benzene reaction.[5]

No evidence was found for H atom displacement occurring in the thiirane reaction or for S atom abstraction occurring in the thiophene reaction. However, S atom abstraction from thiophene involves the formation of the very weakly bound cyclobuta-1,3-diene molecule

$$O(^3P) + C_4H_4S \rightarrow SO(^3\Sigma^-) + C_4H_4 \qquad (4)$$

and is estimated[13] to be strongly endoergic, $\Delta D_0 = -76$ kJ mol^{-1}. Hence, the hypothetical pathway of eq 4 is energetically inaccessible in these experiments.

Discussion

The approach of the O(^{3}P) atom to the S atom of the thiirane molecule involves overlap of the O atom p orbital with the lone pair orbital of the S atom, corresponding to a pyramidal configuration[14] about the S atom as shown in Figure 7. On the triplet ^{3}A″ potential energy surface, repulsion will be invoked in both the C−S bonds as the π orbitals of the C_2H_4 moiety overlap with the π orbitals of the SO moiety, leading to the formation of C_2H_4 and SO($^3\Sigma^-$) reaction products. However, on the singlet ^{1}A′ potential energy surface, the pyramidal configuration[15] corresponds to the thiirane 1-oxide molecule, which is estimated[16,17] to be stable by ~90 kJ mol^{-1} with respect to reaction products. Consequently, the triplet potential energy surface which declines steeply in the exit valley is underlain by the singlet potential energy surface which correlates with the electronically excited singlet states of the reactant O(^{1}D) atom and the SO($^1\Delta$) product molecule.[18] Hence, the triplet potential energy surface is intersected by the singlet potential energy surface in both the entrance and exit valleys as shown in Figure 8. Indeed, infrared multiphoton dissociation of thiirane 1-oxide molecules follows a spin-forbidden pathway[16,17] to form the SO($^3\Sigma^-$) product over the potential energy barrier shown in Figure 8, corresponding[19] to an activation energy $E_a \sim 150$ kJ mol^{-1}.

This situation is illustrated by the molecular orbital diagram for the thiirane ring of the O + C_2H_4S transition state shown in Figure 7. Bonding is assumed to arise from the overlap of the antibonding π* orbitals of the SO radical which are mainly confined to the S atom and the C atom π orbitals of the C_2H_4 moiety. In the case of the singlet thiirane 1-oxide molecule only the lowest two molecular orbitals are occupied, $1a'^2 1a''^2$, resulting in two electron pair S−C bonds and no net C−C π bonding. However the triplet transition state promotes one electron to the higher 2a′ orbital $1a'^2 1a''^1 2a'^1$, resulting in a reduction of the C−S bonding by one half and the creation of C−C π bonding of equal notional strength. Consequently, the concerted rupture of the thiirane ring is expected to involve simultaneous weakening of both C−S bonds and strengthening of the C−C π bonding. The reaction of O atoms with thiirane molecules results overall in the formation of a new π bond of the C_2H_4 molecule as well as the bonding of the SO($^3\Sigma^-$)

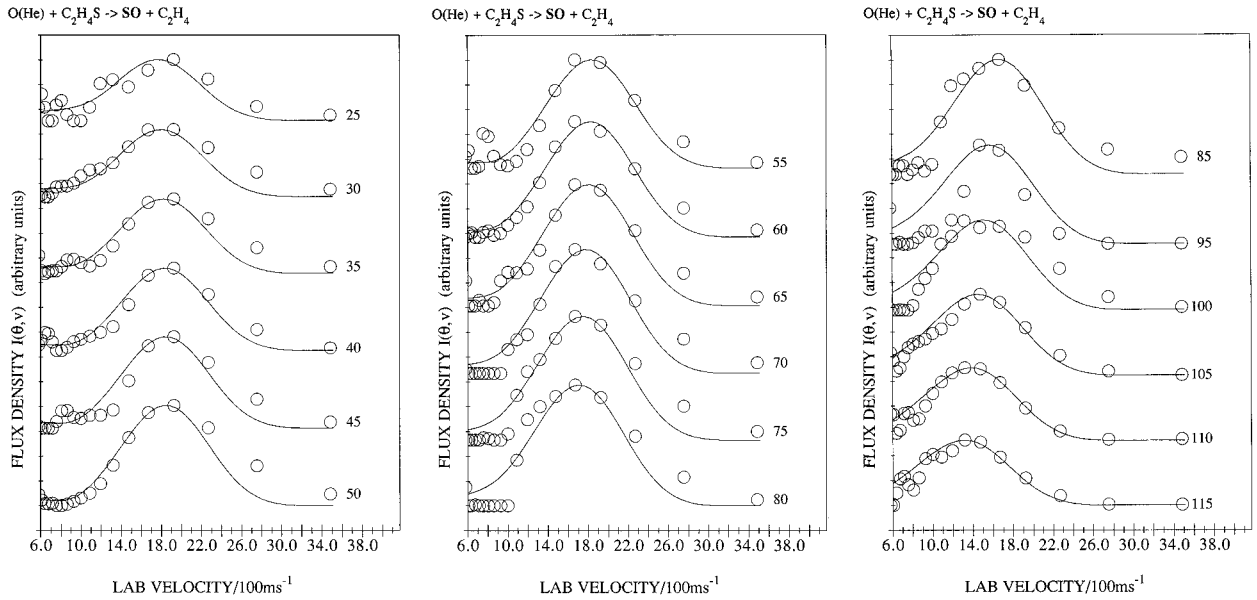

Figure 3. Laboratory velocity distributions (flux density) of reactively scattered SO from O + C_2H_4S at an initial translational energy $E \sim 41$ kJ mol^{-1}. The solid line shows the fit of the stochastic kinematic analysis.

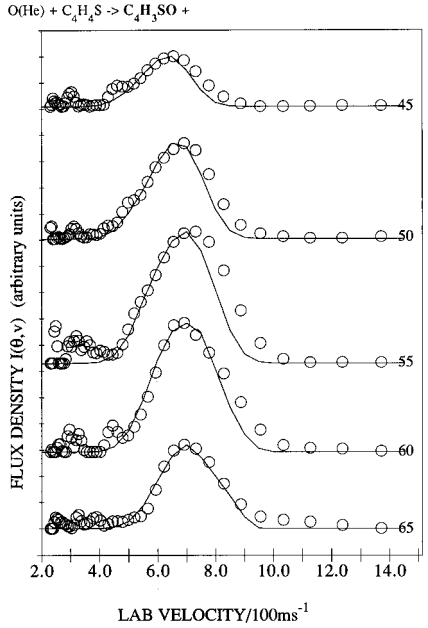

Figure 4. Laboratory velocity distributions of reactively scattered OC_4H_3S from O + C_4H_4S at an initial translational energy $E \sim 37$ kJ mol^{-1}.

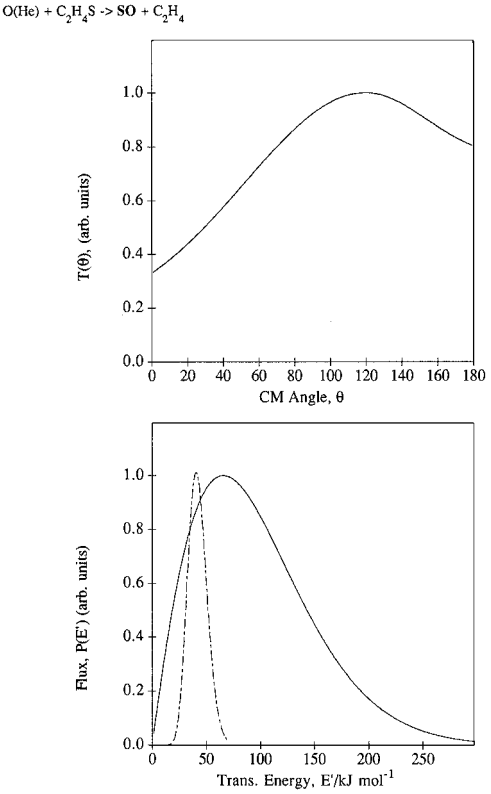

Figure 5. Angular function $T(\theta)$ and translational energy distribution $P(E')$ for O + C_2H_4S at an initial translational energy $E \sim 41$ kJ mol^{-1}. The dashed energy curve shows the distribution of initial translational energy.

molecule. Both the ground $1a'^2 1a''^2$ and first excited $1a'^2 1a''^1 2a'^1$ singlet states correlate with the electronically excited SO($^1\Delta$) state.

The observed SO reactive scattering corresponds to direct dynamics over the triplet potential energy surface arising from collisions at small impact parameters with repulsion between the reaction products,[7] giving SO($^3\Sigma^-$) molecules recoiling in the backward hemisphere. The bent configuration of the transition state on the triplet potential energy surface as shown in Figure 7 results in the SO angular distribution peaking[14] away from the backward direction $\theta = 180°$, and repulsion between reaction products results in a peak product translational energy $E'_{pk} \sim 66$ kJ mol^{-1}. However, the average product translational energy corresponds to only a fraction $f' \sim 0.31$ of the total energy available to reaction products, while the laser-induced fluorescence measurements[1] show only a fraction (~0.16) being disposed into vibrational and rotational excitation of the SO($^3\Sigma^-$) product molecules. Hence, a major fraction (~0.5) of the total available energy must be disposed into vibrational excitation of the C_2H_4 product molecules. This corresponds to structural changes of the C_2H_4 moiety with the H atoms moving from tetrahedral to planar configurations about the C atoms and a contraction ~0.15 Å in the C−C bond length, as the three-membered ring of the thiirane reactant molecule changes to the C=C double bond of the ethene product molecule. The inverted SO($^3\Sigma^-$) vibrational state distribution[1] and high vibrational excitation of C_2H_4 products suggest a concerted rupture of both C−S bonds of the three-membered

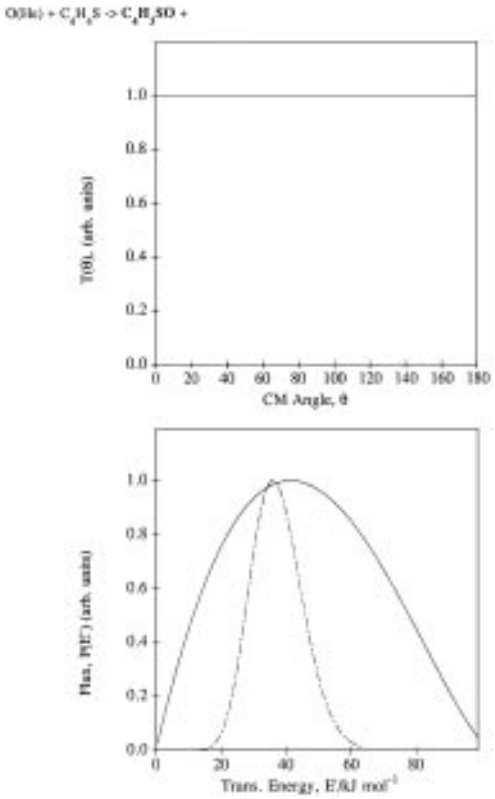

Figure 6. Angular function $T(\theta)$ and translational energy distribution $P(E')$ for O + C_4H_4S at an initial translational energy $E \sim 37$ kJ mol^{-1}.

TABLE 2: Reaction Energetics (kJ mol^{-1}), Initial Translational Energy E, Peak Product Translational Energy E'_{pk}, Average Product Translational Energy E'_{av}, and Reaction Exoergicity ΔD_0

reaction	E	E'_{pk}	E'_{av}	ΔD_0
O + C_2H_4S → SO + C_2H_4	41	66	96	265 ± 10
O + C_4H_4S → OC_4H_3S + H	37	40	45	67 ± 10

thiirane ring leading to a rapid recoil of the reaction products, as indicated by the backward scattered SO angular distribution.

The mass spectrometric measurements of the present experiments do not distinguish between the SO($^3\Sigma^-$) ground state and the SO($^1\Delta$) electronically excited state of the SO reaction product. The low excitation energy $T_e = 70$ kJ mol^{-1} of the SO($^1\Delta$) state[18] implies that only the high-energy tail of the product translational energy distribution of Figure 5 can be identified with SO($^3\Sigma^-$) on energetic grounds. However, intersystem crossing to the singlet potential energy surface would involve the formation of the stable thiirane 1-oxide molecule and result in a longer-lived collision intermediate than is indicated by the direct dynamics observed in these experiments. Thus, reaction appears to be confined to the triplet potential energy surface with little evidence for intersystem crossing to the underlying singlet potential energy surface.

The SO reactive scattering from O + C_2H_4S closely resembles that from the O + OCS reaction,[7] where the SO product has a conical angular distribution in the forward hemisphere peaking at $\theta_{pk} \sim 70°$, but there is very little vibrational excitation of the CO product molecule. DIPR model calculations[7] indicate that the SO angular distribution arises from broadside addition of the O atom to the C═S double bond of the OCS molecule. The more backward peaked angular distribution of the O + C_2H_4S reaction in Figure 5 may be attributed to a less strongly bent addition of the O atom to the electron lone pair orbital of the S atom of the pyramidal OSC_2H_4 transition state of Figure 7. The vibrational excitation of the C_2H_4 product molecule

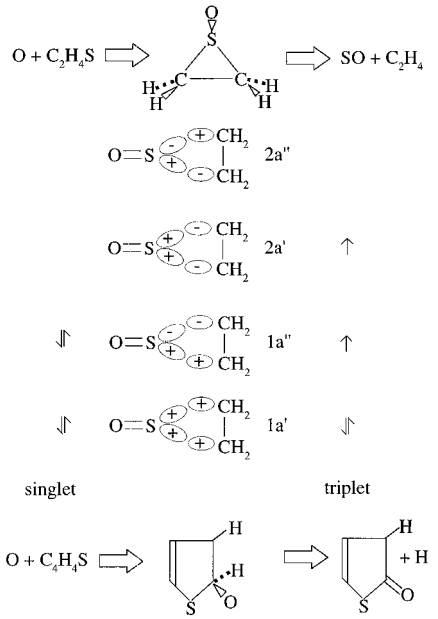

Figure 7. Reaction intermediates on the triplet potential energy surfaces for the O(^{3}P) + C_2H_4S and C_4H_4S reactions. Schematic molecular orbital diagram for the thiirane ring of the O + C_2H_4S transition state. Orbital symmetries relate to reflection in the plane containing the O and S atoms and the center of the C_2H_4 moiety.

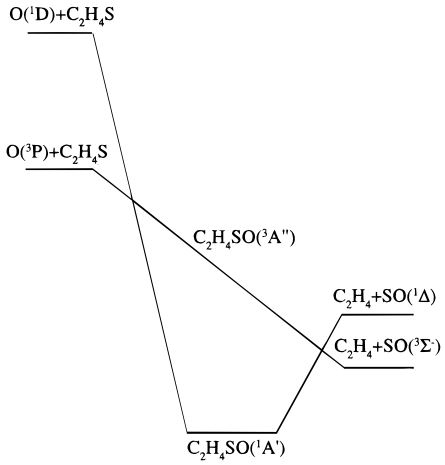

Figure 8. Potential energy profiles for the ^{3}A″ triplet and ^{1}A′ singlet potential energy surfaces of the O(^{3}P) + C_2H_4S reaction. Symmetry species refer to reflection of the electronic wave function in the plane containing the SO bond and the center of the C_2H_4 moiety.

arises from the C−C π bond formation during rupture of the C_2H_4S ring, in contrast to the CO bonding of OCS which undergoes little change, with the CO bond length decreasing by only ∼0.03 Å in forming the CO product molecule.

In contrast to the thiirane reaction, addition of the O(^{3}P) atom to the C═C double bond of the thiophene molecule results in the formation of a stable triplet OC_4H_4S radical as shown in Figure 7. This constitutes a persistent collision complex with a lifetime longer than its rotational period before the H atom adjacent to the O atom becomes displaced to form the reaction products. The product translational energy distribution of Figure 6 indicates that the H atom displacement involves a potential energy barrier, which disposes a substantial fraction of the total available energy into product translation. Hence, the thiophene reaction follows a similar mechanism to that of the benzene molecule,[5,6] but no evidence was found for the formation of a stable OC_4H_4S adduct following intersystem crossing to the underlying singlet potential energy surface, as has been observed[5] for the benzene reaction. Hence, the thiirane and

thiophene reactions both follow the most exoergic pathways over the triplet potential energy surfaces under the single-collision conditions of these experiments.

Acknowledgment. Support of this work by EPSRC and the European Commission is gratefully acknowledged.

References and Notes

(1) Ravichandran, K.; Gong, Y.; Wu, F.; Weiner, B. R. *Chem. Phys. Lett.* **1996**, *252*, 348.
(2) Lee, J. H.; Timmons, R. B.; Stief, L. J. *J. Chem. Phys.* **1976**, *64*, 300.
(3) Lee, J. H.; Tang, I. N. *J. Chem. Phys.* **1981**, *75*, 137.
(4) Acheson, R. M. *Chemistry of Heterocyclic Compounds*; Interscience: New York, 1960.
(5) Gonzalez Urena, A.; Hoffmann, S. M. A.; Smith, D. J.; Grice, R. *J. Chem. Soc., Faraday Trans. 2* **1986**, *82*, 1537.
(6) Sibner, S. J.; Buss, R. J.; Casavecchia, P.; Hirooka, T.; Lee, Y. T. *J. Chem. Phys.* **1980**, *72*, 4341.
(7) Rochford, J. J.; Powell, L. J.; Grice, R. *J. Phys. Chem.* **1995**, *99*, 15369.
(8) Wang, J. J.; Smith, D. J.; Grice, R. *J. Phys. Chem.* **1996**, *100*, 6620.
(9) Wang, J. J.; Smith, D. J.; Grice, R. *J. Phys. Chem.* **1996**, *100*, 13603.
(10) Gorry, P. A.; Grice, R. *J. Phys. E.* **1979**, *12*, 857.
(11) Nowikow, C. V.; Grice, R. *J. Phys. E* **1979**, *12*, 515.
(12) Entemann, E. A.; Herschbach, D. R. *Discuss. Faraday Soc.* **1967**, *44*, 289.
(13) Pedley, J. B.; Naylor, R. D.; Kirby, S. P. *Thermochemical Data of Organic Compounds*, 2nd ed.; Chapman and Hall: London, 1986.
(14) Zhu, Z. Z.; McDouall, J. J. W.; Smith, D. J.; Grice, R. *Chem. Phys. Lett.* **1992**, *188*, 520.
(15) Mitchell, R. W.; Hartmann, F. A.; Merritt, A. J. *J. Mol. Spectrosc.* **1969**, *31*, 388.
(16) Gross, H.; He, Y.; Quack, M.; Schmidt, A.; Seyfang, G. *Chem. Phys. Lett.* **1993**, *213*, 122.
(17) Gross, H.; He, Y.; Jeitzinger, C.; Quack, M.; Seyfang, G. *Ber. Bunsen-Ges. Phys. Chem.* **1995**, *99*, 358.
(18) Bielefeld, M.; Elfers, G.; Fink, E. H.; Kruse, H.; Wildt, J.; Winter, K.; Zabel, F. *J. Photochem.* **1984**, *25*, 419.
(19) Hartzell, G. E.; Page, I. N. *J. Am. Chem. Soc.* **1966**, *88*, 2616.